Efficiency and Forward Voltage of Blue and Green Lateral LEDs with V-shaped Defects and Random Alloy Fluctuation in Quantum Wells

Cheng-Han Ho, 1 James S. Speck, 2 Claude Weisbuch, 2, 3 and Yuh-Renn Wue1, 4,

(Received 20 September 2021; revised 6 December 2021; accepted 21 December 2021; published 25 January 2022)

For nitride-based blue and green light-emitting diodes (LEDs), the forward voltage Vror is larger than expected, especially for green LEDs. This is mainly due to the large barriers to vertical carrier transport caused by the total polarization discontinuity at multiple quantum well and quantum barrier interfaces. The natural random alloy fluctuation in quantum wells has proven to be an important factor reducing *Vro*,—However, this does not suffice in the case of green LEDs because of their larger polarization-induced barrier. V-shaped defects (V-defects) have been proposed as another key factor in reducing *Vro*, to allow lateral injection into multiple quantum wells, thus bypassing the multiple energy barriers incurred by vertical transport. In this paper, to model carrier transport in the whole LED, we consider both random-alloy and V-defect effects. A fully two-dimensional drift-diffusion charge-control solver is used to model both effects. The results indicate that the turn-on voltages for blue and green LEDs are both affected by random alloy fluctuations and the V-defect density. For green LEDs, Vror decreases more due to V-defects, where the smaller polarization barrier at the V-defect sidewall is the major path for lateral carrier injection. Finally, we discuss how the V-defect density and size affects the results.

DOI: 10.1103/PhysRevApplied.17.014033

I. INTRODUCTION

Blue nitride-based light-emitting diodes (LEDs) with phosphor have become the major white-light source. However, high-efficiency or micro-LED display applications require green- and red-light sources and, for ultimate efficiency, white-light lamps based on RGB color mixing. Currently, the peak internal quantum efficiency (IQE) of blue LEDs is over 90% at a current density of 1-10 A/cm² [1]. However, the IQE of green LEDs remains low, which is likely due to the strong quantum-confined Stark effect induced by the polarization charge and the large defect density [1-3]. In addition, the forward voltage *Vro*, of green LEDs also exceeds the expected 2.3 V [4], which also limits the wall-plug efficiency.

Group Ill-nitrides in the common (000 I) orientation have polarization-induced barriers at the (ln, Ga)N/GaN quantum well (QW) or quantum barrier (QB) interface due to spontaneous and piezoelectric polarization differences between the well and barrier materials [5]. The polarization discontinuity at the QW-QB interface results in significant electric fields in the QWs and QBs--often referred to as

"piezofields." For green LEDs, the polarization discontinuity at the QW-QB interface increases due to the increased lattice mismatch between the (In, Ga)N and GaN layers.

The influence of polarization-induced barriers has been discussed in many studies [4,6,7] where carriers are easily blocked by the extra potential barrier. Our previous studies of blue LEDs [8,9] show that fluctuations in indium composition provide extra paths for carrier injection. Including random indium composition fluctuations in models thus helps to explain the lower Vror in blue LEDs compared with models without fluctuations [10,11].

To further reduce Vror in situations with larger barriers, such as in green LEDs, it is important to either reduce the polarization field or find an alternative way to inject carriers. The most significant method is by controlling the V-shaped defect (V-defect) opened at the (In, Ga)N/GaN multiple quantum well active regions to provide an alternative way to inject carriers. Most V-defects are the result of dislocation lines that form under certain growth conditions [12-14]. Unlike the threading dislocation (TD) centers, which are typical nonradiative centers, the inclined sidewalls of V-defects reportedly assist carrier injection into QWs [15--17]. Since both random alloy fluctuations and V-defects provide concurrent paths for carrier injection,

Graduate Institute of Photonics and Optoelectronics, National Taiwan University, Taipei 10617, Taiwan

²Materials Department, University of California, Santa Barbara, California 93106, USA

³Laboratoire de Physique de la Matiere Condensee, Ecole Polytechnique, CNRS, IP Paris, Palaiseau Cedex 91128, France

⁴Electronic and Optoelectronic System Research Laboratories, Industrial Technology Research Laboratories, Hsinchu, Taiwan

yrwu@ntu.edu.tw

it is important to model both effects in carrier injection simultaneously. The importance of considering both mechanisms is obvious as the paper leads to the conclusion that random alloy fluctuations suffice to lead to efficient low-voltage injection in blue LEDs while V-defects are needed to achieve this in longer wavelength LEDs in the green spectral range.

Given that V-defects play an important role in carrier injection, it is important to understand the role of random alloy fluctuations and of V-defects in carrier injection. The V-defect and random alloy effects may be simulated separately in three-dimensional simulations [8,15]. On the one hand, V-defects range from a few hundred nanometers in size to the micrometer scale, allowing for large mesh sizes. On the other hand, random alloy fluctuations occur on a scale of a few nanometers, requiring mesh elements to be as small as possible to account for such small-scale fluctuations. Including both effects in a three-dimensional simulation requires unreasonable computer memory (> a few terabytes) and computing times. However, to understand the influence of random alloy fluctuation and the V-defect on the efficiency of LEDs, especially for green LEDs, it is essential to include both effects simultaneously. Recent results on the lateral carrier diffusion [18] in a OW show that the random alloy fluctuations strongly limit carrier diffusion. Hence, if the carriers are only injected through V-defects, the current spreading to the whole QW area from the V-defect will be limited, which is observed without considering random alloy fluctuation. Furthermore, the improvement in tum-on voltage induced by V-defects, critical to the wall-plug efficiency, can be jeopardized by the adverse action of the threading dislocation within the Vdefects as nonradiative centers on the IQE. The balance between the reduction of *Vro*, by increasing the V-defect density and the simultaneous decrease in IQE must be explored. A compromise to the present difficulties ofthreedimensional (3D) simulations is to work on 2D simulations that include random alloy fluctuations and V-defects. Some issues might be missed in the 2D model, such as the estimation of carrier quantum confinement effects occurring in 3D. This may affect the estimation of carrier overlap in random alloy fluctuating potentials. The V-defect filling factor of 2D and 3D models may not be equal and needs some translation. However, the 2D model enables us to calculate the whole LED structure, including the current crowding effect. This helps us to understand the simultaneous influences of the V-defect density and random alloy fluctuation to Vro, and IQE. In this paper, we discuss the influence of V-defects and random alloy fluctuations with such an alternative 2D model.

The V-defects may be controlled by tuning the growth conditions. Often, V-defects are formed in the widely used (In, Ga)N/GaN short periodic superlattice that is grown before growing active (In, Ga)N/GaN QWs [19]. The general V-defect density is about I x 10^7 cm- 2 \sim

5 x 10⁸ cm⁻², and the typical diameter is about 30-250 nm for five QWs in blue LEDs [12-14,19]. Hence, in this paper, we cover the V-defect density from O to about 6.25 x 108 cm⁻². Furthermore, V-defects form an inverted hexagonal pyramid with six inclined {10I1} semipolar sidewalls [20]. Studies show that the indium composition inc-plane QWs is greater than in the inclined QWs in the V-defect region [21]. Therefore, the bandgap of QWs in the inclined sidewall of V-defects is larger than the bandgap of QWs in the c plane. The polarization discontinuity between the semipolar {10**I1**} (ln,Ga)N sidewall QW and QB is much smaller than the c-plane QW and is in the opposite direction [22]. Thus, holes can be injected into the OWs in the c plane through the sidewall V-defect QWs with lower barrier potentials[23]. The additional paths provided decrease Vror and increase the carrier-injection efficiency [24-26]. However, V-defects form at TDs, and a high density of nonradiative centers at the center of V-defects could be a drawback. Thus, the density and diameter of the Vdefects in the LED should be optimized to minimize this counteracting effect [27].

In this paper, we use simulations to investigate how random fluctuations and V-defects affect (ln, Ga)N-based LEDs. As mentioned above, computer-memory limitations oblige us to use 2D simulations with fluctuations instead of 3D simulations. In 2D simulations, the size of the simulated structure may be increased to the micron scale to approach the real device structure of LEDs. In the following, we discuss the 2D structure with different V-defect densities and diameters (lateral size). The forward voltage Vr_0 and efficiencies (electrical and IQE) are discussed and explained by the interplay between lateral carrier injection through the V-defect sidewalls and subsequent carrier diffusion within the planar QW regions.

II. METHODOLOGY

To simulate random alloy fluctuations in devices, we use an in-house-developed 2D drift-diffusion charge control solver to determine the electrical carrier distribution, recombination rates, and other properties. First, to account for the random alloy fluctuations and V-defects, we construct a mesh for a device with a V-defect. The mesh size at the QW region is 0.5 nm in the x direction and 0.1 run in the x direction. The mesh size is larger in the x and x layers to save computer memory. We then use a random number generator to create the random atom distribution in the alloy regions [28] and subsequently use Gaussian averaging to assign the local indium composition in the QWs [29-31].

Figure 1 shows the indium composition fluctuations in the QWs, where the bandgap depends on the indium composition. Note that, in the 2D simulation, we cannot calculate the real strain distribution with a strain solver because we have neglected the third dimension. Thus,

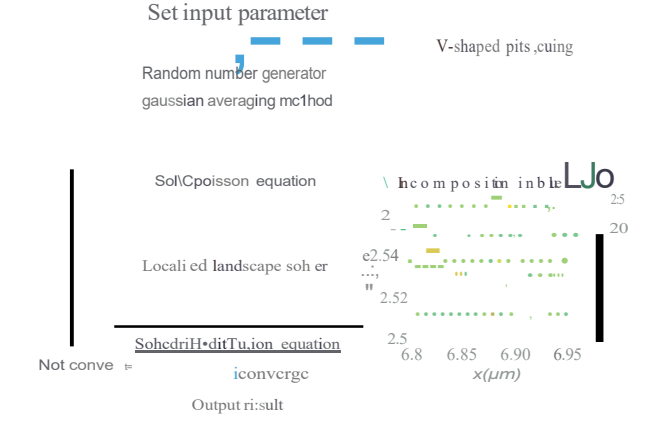


FIG. I. Flow chart of the simulation model. The mesh with V-defectshapes is put in the simulation program. The random alloy map is generated by using a random number generator and then put in the solver to realize convergence after the required number offeedback loops. The right panel shows the indium composition map in the MQWs.

fully compressive strain is assumed when calculating the lattice size of the GaN buffer layer based on the local indium composition. We then calculate the local material parameters such as bandgap, conduction- and valence-band energies, polarization according to the local indium composition, and strain state. In addition, we use the localization landscape (LL) model [29,32,33] shown in Eq. (2) below instead of the Schrodinger equation solver to obtain the effective quantum potential seen by the carriers [31].

A. Methodology of analyzing the two-dimensional solver

To simulate the 2D Poisson, drift-diffusion, and LL equations, the following equations were used:

$$\mathbf{V} \cdot (\text{sVcp}) = q(n - p + N; -Nj; \pm ppo 1), \tag{1}$$

[-
$$\underline{\underline{V(m, V)}}$$
 | $Ec, v Jue, h = 1,$ (2)

$$n \stackrel{\text{d}}{=} O O O S(E) \underset{\text{I} + \exp[(E - EFn)/knTJ)}{\text{I}} dE, \quad (3)$$

$$p = 1 \frac{\text{LDOS(E)} - - - - dE}{\text{I} + exp[(EFp - E)/knTJ}, (4)}$$
$$J_{n,p} = /I_{,n,p(n,p)}VEF''.fl'$$
 (5)

$$\frac{1}{2}V(Jn,p) = Rn,p - Gn,p,$$
(6)

$$R = R_{SRH} + B_0 np + C_0 (n^2 p + np^2), \tag{7}$$

In these equations, cp is the electrostatic potential in the structure, n and p are the free-electron and hole concentrations, and Ni and N''J are the ionized acceptor and donor concentrations determined by the ionization energy (and

position in the junction and junction electric field), respectively. Here Ppol is the polarization charge that has been computed from the divergence of the total polarization, and 1/ue and 1/ulz are the effective quantum potentials of electrons and holes calculated by the LL equations [29,33], respectively.

First, we calculate *cp* by using the Poisson equation (1) and obtain the local band extrema Ee and Ev through the local cp and alloy composition. Then, the LL equations (2) are solved to yield ue and uh and the effective quantum potentials 1/ue and 1/ulz. The carrier distributions are calculated by using Eqs. (3) and (4), the effective quantum potentials 1/ue and 1/u,,, and the quasi-Fermi levels EFn and EFp. Finally, we determine EFn and EFp from Eqs. (5) and (6). The recombination rate is given by Eq. (7), and includes radiative recombination (IQE), Auger recombination, and Shockley-Read-Hall (SRH) recombination. Bo is the radiative recombination coefficient and Bonp denotes the radiative recombination rate. Co is the Auger recombination rate coefficient. The term with C₀ is the recombination of three particles, either directly or mediated by phonons [34]. Equation (8) is the SRH recombination equation, where $\le n$ and $\le p$ are the nonradiative carrier lifetimes of electrons and holes, respectively.

Next, we construct the mesh according to the position in the structure; each mesh point has different parameters. To simulate V-defects in the structure, the mesh is readjusted according to the V-defect diameter and density. Finally, these equations are solved self-consistently. Figure 1 shows a detailed flowchart of the simulation.

B. Device structures and parameters

To discuss the V-defect, we analyze the blue and green LEDs with the structure shown in Fig. 2(a). The chip lateral size is 11μ , m and the region of multiple quantum wells (MQWs) is 10μ , m wide, which is also defined as the total region. Since our mesh element size is quite small compared to the the deprecation we which about the structure of the the deprecation which about the structure of the the deprecation which about the structure of the the deprecation which are the structure of the the structure of the structu

of memory to run the 2D simulation. The p contact (in common p-side LEDs, this layer is made from indium tin oxide) is about 9 μ ,m wide at the center of the active region, and the n pad is about I μ ,m wide.

For the blue and green LEDs, we consider a MQW LED with a 0.14 μ ,m top p-GaN layer doped at 3 x 10¹⁹ cm⁻³,

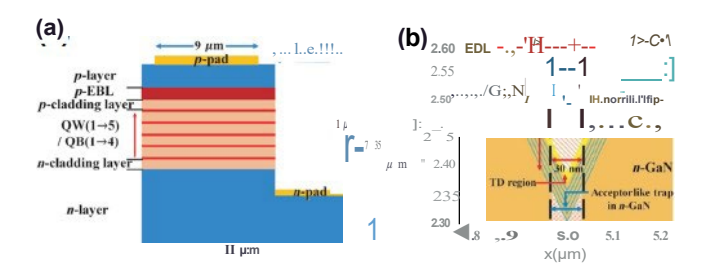


FIG. 2. (a) Simulated structure of the lateral LED. (b) Definition of parameters for the V-defect structure.

a p-(Al, Ga)N electron blocking layer (EBL) and p-GaN cladding layer both doped at 2 x 10¹⁹ cm-³, five QWs and four QBs between the QWs are unintentionally doped n type at 1 x 10¹⁷ cm⁻³, one 10 nm n-cladding layer and then a 2.5 μ ,m n-GaN layer doped at 5 x 10^{18} cm- 3 . The doping density of the n-type cladding layer is 1.0 x 10^{19} cm^{-3} . For the green LED, the first two QBs are ndoped at 1.0 x 10¹⁸ cm⁻³ to partially screen the piezoelectric field for better vertical carrier injection. We also ran a simulated case without doping in the first two QBs (and with no V-defects) for comparison. In addition, "n and r:Pfor the blue and green LEDs are 1 00 and 10 ns, respectively, because the green LED has a higher In content in the (ln, Ga)N than the blue LED and thus a lower growth temperature, which leads to a higher density of SRH centers in the real device. The detailed parameters of the structures are shown in Table I. For the blue LED, the average indium composition in the OWs is 13% (In_{0 13}Gao.81N). For the green LED, the average indium composition in the QWs is 22% (Ino.22Gao.1&N). Additionally, alloy fluctuations in the (In, Ga)N layers are included in both the blue and green LEDs. The Bo is 2 x 10^{-11} cm³/Vs and the Co is 2 x 10-31 cm⁶/Vs. These two parameters are not changed in the simulation since we focus on V-defect and random alloy fluctuation influences. The influence of overlap due to the different quantum-confined Stark effect and disorder is included in the term of $n(r) \times p(r)$.

TABLE II. Trap parameters in the threading dislocation (TD) center.

Туре	Trap density (1/cm ³)	Trap < <i>n</i> ,< <i>p</i> (ns)	E, below Ee (eV)
Donorlike	1 x 10 ¹⁸	1.01	1.14
Acceptorlike	1x 10 ¹⁸	0.38	2.5

Figure 2(b) shows the geometrical definition of Vdefects, where H and D are the depth and diameter of the V-defect, respectively. We use these parameters in the following discussion. The region between the vertical black dotted lines corresponds to the TD along the direction {0001} with a 30 nm width at the center of the V-defect, and the V-defect sidewall OWs are inclined about 60° according to both transmission electron microscopy (TEM) and scanning TEM [35,36], which is consistent with early work showing that the sidewalls are {IO11} planes. In addition, the thickness of the c-plane QWs is 3 nm. The inclined sidewall QW is also 3 nm thick in the z direction, which corresponds to a thickness of 1. 73 nm (3 nm x cos 60°) along the normal to the inclined plane [37]. The indium composition in the inclined QWs depends on the composition in c-plane OWs. For example, for blue LEDs, the indium composition of inclined QWs is 8% [38,39]. For green LEDs, the indium composition in the inclined QWs is about 16% [40]. In addition, the TDs are defects induced by the lattice and chemical mismatch between the sapphire substrate and GaN [41,42]. Thus, we include TDassociated trap states in the TDs regions, which trap either electrons or holes and are shown as the cross-hatched areas in Fig. 2(b). The density of TD-associated trap states is about 1 x 10¹⁸ cm-3, corresponding to one trap state per c translation along the dislocation line within the 30 nm diameter TD ranges [43,44]. The trap energy level (E_{I}) is 1.14 eV below Ee for donorlike traps and 2.5 eV below Ee for acceptorlike traps, as shown in Table II. The trap lifetimes are also given in Table II [44].

TABLE I. Basic parameters of blue and green LEDs.

Area	Material	Thickness (nm)	Doping blue, green (1018 cm-3)	Ea (meV)	<i>e,h</i> mobility (cm²/V s)	< <i>n</i> ,< <i>p</i> blue (ns)	< <i>n</i> ,< <i>p</i> green (ns)
player	p-GaN	140	30,30	180	100,5	100	10
p EBL	p-(Al,Ga)N	20	20,20	264	100,5	100	10
p cladding layer	p-GaN	10	20,20	180	100,5	100	10
QW(3,4,5)	n-(ln,Ga)N	3	0.1, 0.1	25	150, 10	100	10
QB(3,4)	n-GaN	10	0.1, 0.1	25	350, 10	100	10
QW(1,2)	n-(ln,Ga)N	3	0.1, 0.1	25	150, 10	100	10
QB(1,2)	n-GaN	10	0.1, I	25	350, 10	100	10
n cladding layer	n-GaN	10	10, 10	25	200, 10	100	10
n layer	n-GaN	2500	5,5	25	200, 10	100	10

III. RESULTS AND DISCUSSION

A. Influence of random alloy fluctuations, V-defects, and threading dislocations for the current path

Figure 3 shows the calculated *Ee* and effective quantum potential 1/ue for the blue and green LEDs, taking into account random alloy fluctuations at a bias voltage V = 3 V. A cross section with minimum potential barrier is chosen for the full curves. They show the best case for carrier transport across the QWs. The dashed curves for disorder-averaged levels show slightly larger barriers. Without considering the random alloy fluctuation, the voltage would be even higher, which has been discussed in Refs. [6,8,31]. Hence we will not discuss the cases with and without random alloy fluctuation. Although Figs. 3(a) and 3(b) show that random alloy fluctuations already change the depth of the OWs for blue LEDs (compare the *Ee* curves with and without fluctuations), the potential barrier induced by the piezoelectric field between QWs is still about 0.4 eV for the blue LED, whose carriers can overcome the barrier through thermal excitation. However, for the green LED, the potential barrier is about 0.7 eV, which strongly impedes carrier transport across the MQWs at the bias V=3 V. While the current density at that bias is a few A/cm² for the blue LED [see Fig. 4(a)], it is negligible in the green LED [Fig. 5(a)]. Thus, even when considering random alloy fluctuations, carriers are hardly injected directly into the c-plane QW for the green LED, despite the large 0.7 V excess voltage. We also observe that the inclusion of the quantum disorder correction through

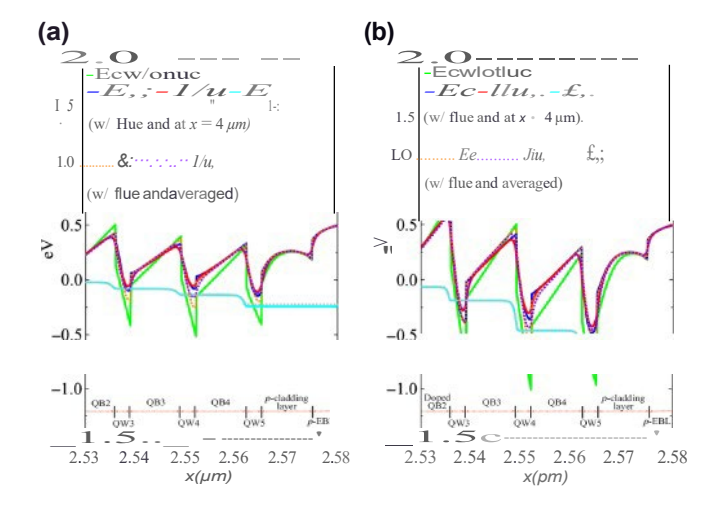


FIG. 3. Cross-section plot for the three top QWs of Ee without fluctuations (Ee w/o flue), Ee with fluctuations (Ee w/l flue), effective potential 1/ue, EFn along the z direction with random alloy fluctuations but without V-defects. Panel (a) shows results for the blue LED and (b) for the green LED. The applied biasis 3 V. The full curves with fluctuations are for the cross section with minimum barrier and the dashed lines are for the fluctuation-averaged potential Ee, 1/ue, and EFn.

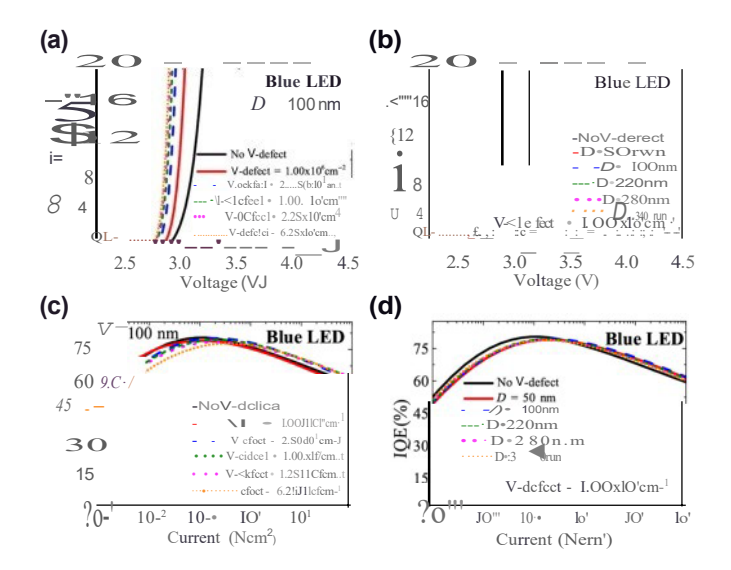


FIG. 4. (a) Voltage versus current for the blue LED at different V-defect densities for a V-defect diameter of D=100 nm. (b) Voltage versus current for the blue LED at different V-defect diameters and a V-defect density of 1 x 10^8 cm-². (c) IQE versus current for the blue LED at different V-defect densities and a V-defect diameter D=100 nm. (d) IQE versus current for the blue LED at different V-defect diameters and a V-defect density of 1 x 10^8 cm-².

the use of the LL theory (thus yielding the effective potential 1/ue) only weakly diminishes the potential barriers, in particular for the green LED. Reducing Vror in these LEDs requires the use of another injection mechanism, namely, injection through V-defects.

We first focus on hole injection through a V-defect. Figures 6(a) and 6(b) show the valence-band potential of blue and green LEDs in a V-defect, respectively. First, in the middle of the V-defect, within ±15 nm of the TD in the *p-GaN* layer region, holes are trapped in the hole traps associated with the TD, which repels holes from the TD center [the repelling potential is shown in a lighter color in the TD region in Figs. 6(a) and 6(b)]. Next, holes transport toward the c-plane QWs through the inclined plane, as shown in Figs. 7(c) and 7(d). Given the position of the electron-injecting region relative to the c-plane QWs, electrons are first injected into the sidewall QWs, from which they diffuse toward the lower-energy c-plane QWs.

Figures 6(c) and 6(d) show the radiative recombination map for the blue and green LEDs at 20 A/cm², respectively. The plot is at log scale. For blue LEDs, recombination occurs throughout the structure as electrons and holes (at least four of the c-plane QWs for holes) are injected vertically [Figs. 7(a) and 7(c)] in the c-plane QWs. For the green LED, while electrons are injected both vertically and through the V-defect [Fig. 7(b)], holes are not injected vertically because of the much larger polarization-induced barrier in the c plane. Holes are therefore injected

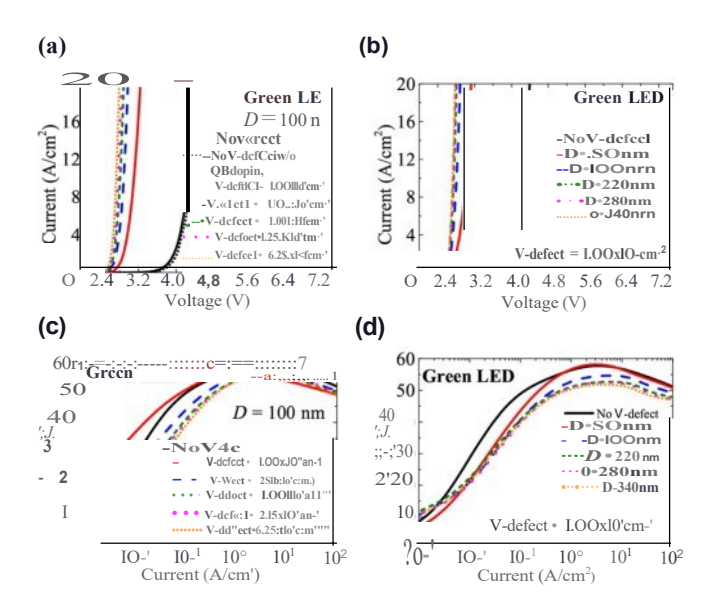


FIG. 5. (a) Voltage versus current for the green LED at different V-defect densities and for a V-defect diameter of D=100 run. (b) Voltage versus current for the green LED at different V-defect diameters and a V-defect density of I x 10^8 cm⁻². (c) IQE versus current density for the green LED at different V-defect densities and for a V-defect diameter of D=100 nm.

(d) IQE versus current for the green LED at different V-defect diameters and a V-defect density of I x 10⁸ cm⁻².

through the V-defect sidewall near which recombination occurs and decays laterally within a characteristic diffusion length. In addition, only two to three c-plane QWs receive holes through the V-defect. Both effects limit the effectiveness of V-defects as a solution to excite the whole volume of the c-plane QWs. For the blue LED, the crowding effect of carriers near V-defects is weaker because holes can still be injected vertically into the whole c-plane area due to random alloy fluctuations. The relative importance of vertical injection versus V-defect injection is discussed in more detail below along with how the V-defect size and density affects *Vro*, and the IQE for blue and green LEDs.

A remarkable phenomenon is seen in Fig. 7: both electrons and holes are preferentially injected into QWs near the middle of the MQW stack, QWS numbers 2, 3, 4 for the blue LED, and QW number 4 for the green LED. This is dominantly due to the peculiarity of hole injection through V-defects. Because of the diminished piezoelectric induced barrier at the sidewall (which is a semipolar plane at 60°), the electrons and holes are more easily injected sideways than vertically, especially for holes, which have a heavier effective mass and lower mobility. Because of the p doping of the last barrier, holes are easily injected in QW5 through the sidewall. Overcoming one more barrier is still relatively easy for holes, compared to the c-plane vertical injection. Holes then first meet electrons in QW4 and recombine there. Why are electrons not injected in QW5? Close inspection of the electron current in Fig. 7(b)

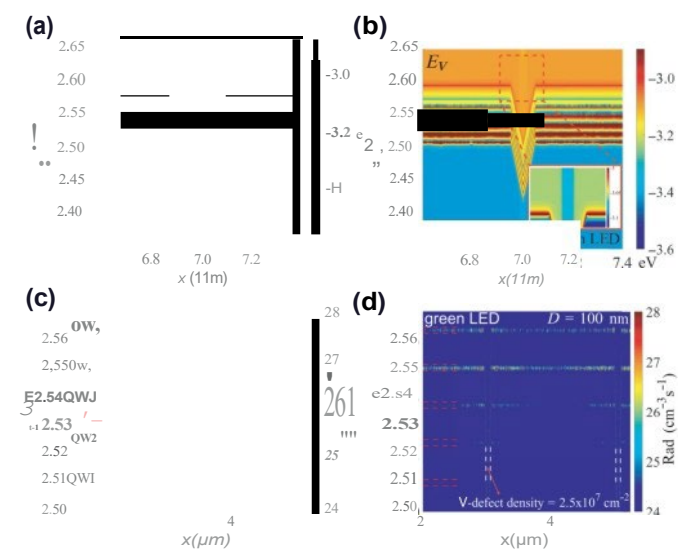


FIG. 6. Valence-band energy and radiative recombination for the blue LED and green LED at a V-defect density of $2.5 \times 10^7 \text{ cm}^{-2}$ and D = 100 run at a current density of $2.5 \times 10^7 \text{ cm}^{-2}$ and D = 100 run at a current density of $2.5 \times 10^7 \text{ cm}^{-2}$. (a) Valence band for the blue LED, (b) valence band for the green LED, (c) radiative recombination for the blue LED at 20 A/cm^2 , and (d) radiative recombination for the green LED at 20 A/cm^2 . The plot of (c) and (d) is at log scale. White dashed lines show the location of V-defects on the *x* axis. Insets in panels (a) and (b) at different color scale emphasize the higher potential energy for holes at the center due to trap charging. The scale color bar ranges from -3.0 eV (red) to -3.1 eV (blue).

for green LEDs shows that they experience a significant energy barrier between the sidewall QWs numbers 4 and 5 (blue color of the barrier). This is due to the nearby p doping inside the V-defect that raises the barrier. The behavior is more significant for the green case, as can be seen in Figs. 7(b) and 7(d), as well as on the recombination current in Fig. 6(d). This is not observed without the V-defect since it is much harder for holes to overcome the large piezoelectric barrier in the c-plane direction, especially in the green case. Then, holes are preferentially injected in QW number 5 where they meet electrons. It is well known that holes in the planar LED case are mainly injected in the QW nearest to the p side in planar MQW LEDs, and this is of course well reproduced in our other simulation papers that include disorder effects without V-defects.

Since carriers are mainly going through V-defects for the green LED, the density of V-defects plays an important role in the LED current-voltage characteristics. Using a high V-defect density to obtain more injection sites, the active c-plane QW area becomes smaller and the carrier density in the c plane increases for the same current. This adversely affects the IQE and droop behavior [45]. Therefore, it is important to discuss in detail how the V-defect density and size affect the LED structure.

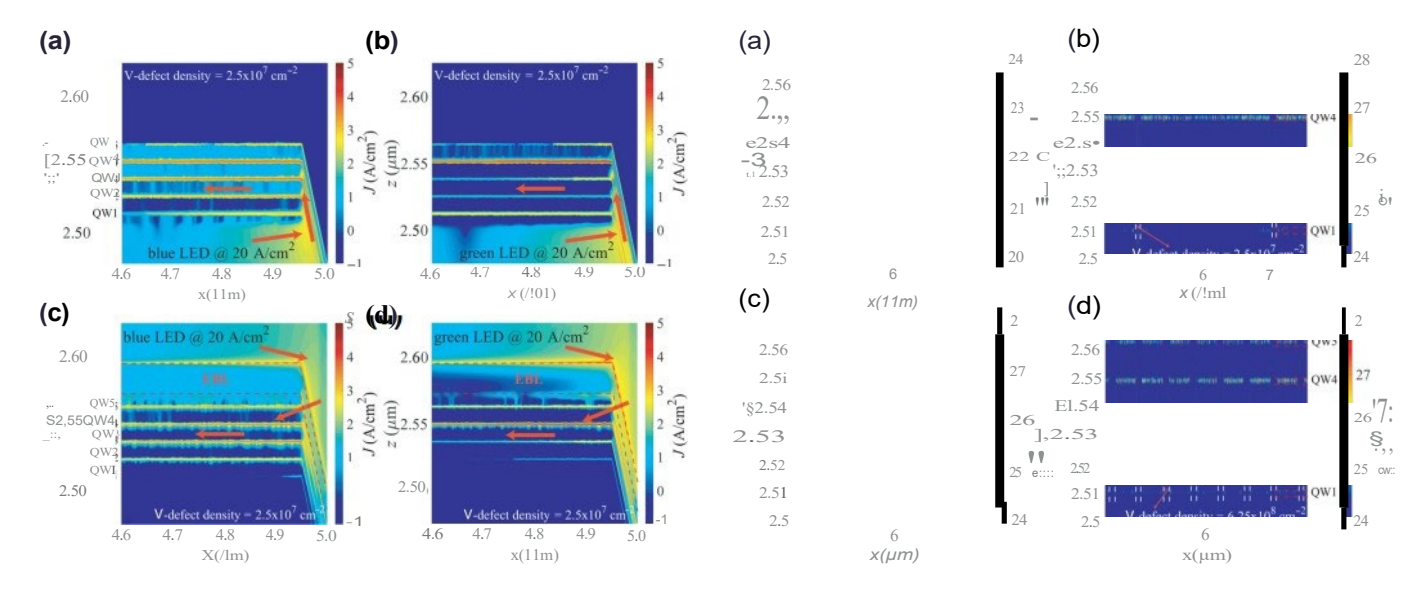


FIG. 7. Current distribution for the blue LED and green LED at a V-defect density of $2.5 \times 10^7 \text{ cm}^{-2}$ and D=100 nm at a current density of $2.5 \times 10^7 \text{ cm}^{-2}$ and D=100 nm at a current density of $2.5 \times 10^7 \text{ cm}^{-2}$. (a) Electron current density $|J\mathbf{n}|$ for the blue LED, (b) electron current density $|J\mathbf{n}|$ for the green LED, (c) holecurrent density $|J\mathbf{p}|$ for the blue LED, and (d) hole current density $|J\mathbf{p}|$ for green LEDs. It is log plot. The vector sense for the electrons [panels (a) and (b)] and holes [panels (c) and (d)] are shown by the red arrows.

B. Influence of V-defects and random alloy fluctuations on/-Vand IQE

The influence of V-defects for the specific lateral LED of Fig. 2 is now discussed for green and blue LEDs. The effects on IQE and Vror of both random alloy fluctuations and V-defects are simulated for different V-defect densities and diameters. We use V-defect densities of 1×10^6 , 2.5×107 , 1×108 , 2.25×10^8 , and 6.25×10^8 cm- 2 and V-defect diameters of 50, 100, 220, 280, and 340 nm.

1. Performance of the blue V-defect LED

We first discuss the dependence of *Vro*, on the V-defect density. Here we define the forward voltage *Vro*, as the voltage needed for a current density of 1 A/cm². Figure 4(a) shows the results for the blue LED structures without and with the V-defects. The V-defect diameter is 100 nm. For the case without V-defects, *Vro*, is about 2.88 V. The maximum density of V-defects is 6.25 x 10⁸ cm-², and *Vro*, for this case is about 2.74 Vat I A/cm², which equates to about zero excess voltage.

For a V-defect density of I x 10⁸ cm-², Fig. 4(b) shows the dependence on V-defect size. The results show that the voltage decreases as the V-defect diameter increases from 50 to 100 nm, but *Vro*, remains constant for the larger V-defect diameters, with all the decrease in *Vro*, already realized at the lateral V-defect size of 50 nm. One factor contributing to this result is that the voltage is already close

FIG. 8. Distribution of the radiative recombination rate for the blue LED with D=100 nm for V-defect densities of (a) 2.5 x 10^7 cm⁻² at a current density of 0.01 A/cm², (b) 2.5 x 10^7 cm⁻² at a current density of 20 A/cm², (c) I x 10^8 cm⁻² at a current density of 20 A/cm², and (d) 6.25 x 10^8 cm⁻² at a current density of 20 A/cm². It is log plot. White dashed lines indicate the location of V-defects on the x axis. The red arrow in panel (b) indicates that the top QW is not injected vertically at low current (bias) and injection occurs through the V-defects. The red dashed lines indicate the QW positions.

to hv/e, leaving little possibility for further reduction of Vro,-

Figure 4(c) shows the IQE of blue LEDs with different V-defect densities; the IQE peak slightly decreases as the V-defect density increases. For high V-defect densities, the IQE peak appears at higher current density. In the low-current-density region (10-3 to 1.0A/cm²), holes are injected mainly through V-defects and electrons are injected vertically through the random alloy fluctuating potential, whereas for higher current density, the higher Vror means that both carriers start to be injected directly from the c-plane QW through the fluctuating potential barriers. Since the V-defect center contains strong nonradiative recombination (NR) centers, carriers injected through V-defects experience more NR.

Figures 8(a) and 8(b) show the radiative recombination for current densities of 10-2 and 20 A/cm², respectively, for blue LEDs at a V-defect density of 2.5 x 10⁷ cm-². At low current density, the top QW shows weak radiative recombination, which means that holes are injected from V-defects due to the diminished piezoelectric field-induced barrier at the sidewall, especially for holes with lower mobility. At high current density, the top QW also emits light because holes are also injected vertically. Thus, at higher current density, the IQE and *Vro*, are less influenced by V-defects and the dislocation region. More QWs

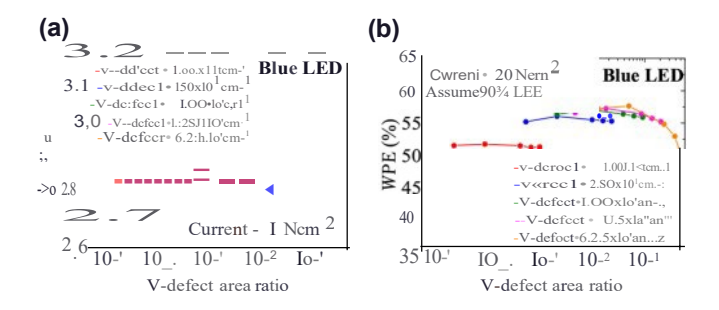


FIG. 9. (a) V-defect region ratio (the V-defect area divided by the chip area) versus tum-on voltage for different V-defect densities at a current density of 1 A/cm² for blue LEDs. (b) V-defect region ratio versus WPE for different V-defect densities at a current density of 20 A/cm² for blue LEDs. The 90% LEE is assumed.

emit light, and the impact of NR diminishes, so all curves regroup.

Figures 8(b)-8(d) show the recombination distribution for different V-defect densities at $J = 20 Ncm^2$. The crowding effect is limited because of vertical injection through random alloy fluctuations but is significant at low V-defect density. Note that if random alloy fluctuations are not considered in the c-plane QW, carrier diffusion extends much further. Then, we do not observe current crowding near the V-defect for the lower V-defect density, making the predicted IQE higher. Increasing the V-defect density diminished the crowding effect and thus moves the peak IQE to a higher current density, although the peak IQE is diminished somewhat because of the increased density of NR centers [Fig. 4(c)]. Figure 4(d) shows the IQE for different V-defect diameters at a V-defect density of 1.0 x 108 cm-2. When the diameter increases, the Vdefect area increases and the active c-plane area decreases. Thus, the IQE decreases with increasing V-defect diameter because of the increased Auger effect, which is consistent with earlier work [15].

To further discuss the joint influence of the V-defect density and diameter on the IQE, we consider the ratio of the V-defect area to the total chip area. Figure 9(a) shows Vror as a function of the V-defect area ratio, where points on a given V-defect density curve correspond to the different Vdefect diameters (50, 100, 220, 280, and 340 nm), which change the V-defect area ratio. At low V-defect area ratio, Vror is affected by both the V-defect area ratio [46] and the V-defect density. This result is attributed to the density being too low, even for large V-defects, so the carriers injected from V-defects need to travel through a long lateral region to inject into the entire QW. 1n addition, the natural alloy potential fluctuations in the QW limit the lateral transport distance of electrons and holes. As a result, carriers become crowded near the V-defect at low V-defect density, so the device performance is strongly limited by the lateral transport distance from the V-defect within the QW [18].

This result is again verified by Figs. 8(b)-8(d). The recombination becomes less crowded when the V-defect density increases. Once the V-defect area ratio grows larger, Vror decreases and then saturates at the expected value near 2.7 V. Another contribution comes from the modified vertical injection due to the presence of V-defects: the fluctuations in the vertical energy barriers induced by the random alloy fluctuations cause some carriers to be directly injected from the c plane in regions with lower barriers. With V-defects, electrons and holes can flow laterally *into* all quantum wells [47]. Once carriers flow into QWs, they screen the polarization-related electric fields so that vertical current injection directly into c-plane QWs increases at lower bias voltage compared with the case without V-defects.

The diameter and density of V-defects also affect the efficiency of the blue LED. Since the optimized performance is decided by wall-plug efficiency (WPE), we estimate the WPE by assuming a 90% light extraction efficiency (LEE), typical of LEDs grown on patterned sapphire substrates. We simulated how the WPE at a fixed 20 Ncm² current density depends on the V-defect area ratio, which corresponds to different diameters and densities of V-defects. The results are shown in Fig. 9(b). Interestingly, the low V-defect densities of 1.0 x 10⁶ and 2.5 x 10⁷ cm-² have a much lower WPE and IQE than the others because the current paths from V-defects to the whole chip area are too long, so the constant injected current of 20 Ncm² becomes crowded near the V-defect region. They also have a higher Vror When the V-defect density exceeds 1.00 x 108 cm⁻², which is within the lateral diffusion length, the carriers are easily injected into the whole active region, diminishing crowding and further canceling the quantum-confined Stark effect. This is also seen in Figs. 8(b)--8(d).

This latter effect helps to increase electron-hole overlap and increase the efficiency. However, the IQE also gradually decreases as the V-defect area ratio further increases because the active volume decreases, and the droop effect starts to dominate at lower current density for larger V-defect area ratios. The conclusion is obvious: it is advantageous (i) to have a high V-defect density so that the V-defect separation is about the lateral carrier transport distance (often referred to as a diffusion length), to inject carriers homogeneously, and (ii) to have small V-defects to minimize nonemitting, unproductive V-defects. The larger V-defect densities also have a smaller *Vror*, but the reduction of Vror saturates as the V-defect density becomes larger than 10^8 cm-². Hence, the WPE reaches a peak at the V-defect ratio around 5%.

2. Performance of the green V-defect LED

For the green LED without V-defects, Vror = 3.83 Vat I A/cm² current density is greater than for the blue LED

[Fig. 5(a)] [4,6]. If we further remove the barrier doping, as indicated by the black dotted line, Vror increases. Despite doping the QB barriers between the MQWs, the polarization barrier induced by the high indium composition is not completely offset. Therefore, V-defects are much more helpful to decrease the tum-on voltage for green LEDs than for blue LEDs. The lowest V-defect density of 1 x 10⁶ cm-² decreases the tum-on voltage to 2.81 V, as shown in Fig. 5(a).

We also simulated different V-defect densities and find that Vror decreases as the V-defect density increases. The different diameters of V-defects are also simulated at a density I x 10^8 cm- 2 , as shown in Fig. 5(b). The results are similar to the blue LED shown in Fig. 4(b). The voltage decreases as the diameter increases and then saturates.

We also calculate IQE versus the V-defect density for D = 100 nm [see Fig. 5(c)]. The results show that different V-defect densities produce different performances. Unlike the blue LED where some carriers are injected from the c plane, in the green LED, most carriers are injected into the planar QWs through the V-defect sidewall, as shown in Figs. 6 and 7. For the lower V-defect density, the IQE peaks slightly higher due to a lower TD density. However, due to greater current crowding, where carriers are crowded in the c-plane QW near V-defects, the droop effect appears at lower current densities, as shown in Fig. 5(c). When the current density increases, additional carriers flow into the whole active QW region for all V-defect densities. Therefore, the IQEs reach a similar value for all V-defect densities, as shown in Fig. 5(c).

Figure 5(d) shows the IQE for different V-defect diameters and for a V-defect density of 1.0 x 10⁸ cm-². For the larger diameters, the V-defect area increases and the active c-plane area decreases. Thus, the IQE decreases as the V-defect diameter increases. To further discuss this, we consider how the performance depends on the V-defect area ratio.

Figure 10 shows the recombination distribution for different current densities and different V-defect densities. Unlike for blue LEDs, a strong crowding effect occurs until the V-defect density exceeds I x 10⁸ cm-², independently of the current density. This again shows that the V-defect density is the dominant factor for carrier injection. As mentioned in the blue case, if the random alloy fluctuation is not considered, the current crowding effect is not observed, which leads to a much higher IQE and the delay of droop behavior.

Figure 11(a) shows Vfor versus the V-defect area ratio and for different V-defect densities. Figure 11(a) shows that the tum-on voltage for green LEDs decreases as the V-defect area ratio increases. In addition, green LEDs have a higher indium composition and a higher polarization-related electric field, so only holes flow into the c plane from V-defects and become crowded at the last QWs, as do electrons [see Fig. 7(b)]. Therefore, the tum-on voltage

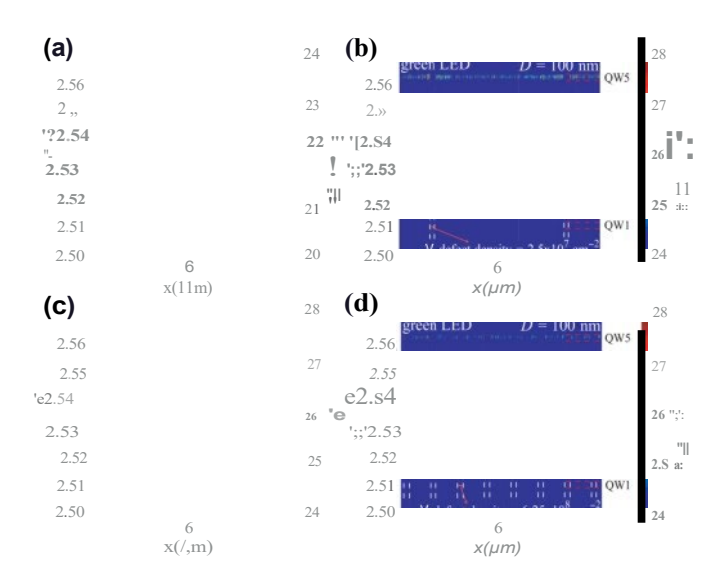


FIG. 10. Distribution of the radiative recombination rate for the green LED at D=100 nm for V-defect densities of (a) 2.5 x 10^7 cm⁻² at a current density of 0.01 A/cm², (b) 2.5 x 10^7 cm⁻² at a current density of 20 A/cm², (c) I x 10^8 cm⁻² at a current density of 20 A/cm², and (d) 6.25 x I 0^8 cm⁻² at a current density of 20 A/cm². The plot is at log scale. Vertical white dashed lines indicate the location of V-defects along the *x* axis.

decreases as the V-defect area ratio increases. This effect influences WPE of the green LED.

Figure 1 l(b) shows how the V-defect area ratio affects the WPE at 20 A/cm². Again a 90% LEE is assumed in estimating the WPE. As mentioned, Vfor decreases as the V-defect area ratio increases, which improves the WPE. At the same V-defect area ratio, a greater V-defect density corresponds to a greater IQE. Because carriers are injected into the QW from V-defects and the diffusion length in the fluctuating QWs is short, the IQE depends much more on the V-defect density than on the V-defect diameter. Combining both effects, the WPE reaches a maximum near 5%

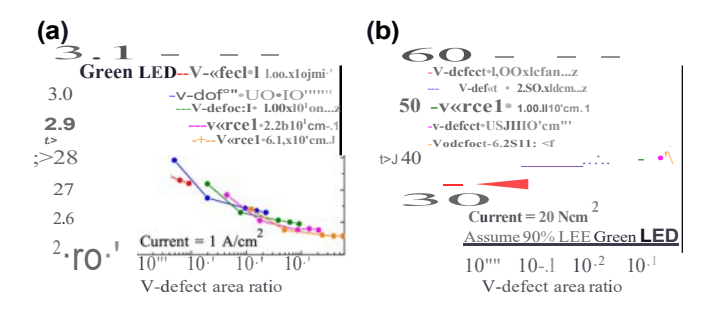


FIG. I I. (a) V-defect region ratio (the V-defect area divided by the chip area) versus turn-on voltage for different V-defect densities at a current density of 1 A/cm² for the green LED. (b) V-defect region ratio versus WPE for different V-defect densities at a current density of 20 A/cm² for the green LED. The 90% LEE is assumed.

V-defect area ratio. For the same V-defect area ratio, a high defect density is preferable in green LEDs since they provide a higher IQE for a similar *Vro*,.

IV.CONCLUSION

In contrast with previous analyses of V-defects [15] in LEDs, we computed the influence of random alloy fluctuations and of the V-defect density and size. Random alloy fluctuations help to inject carriers vertically, whereas weak polarization-related electric fields in the inclined sidewalls of V-defects provide an alternative path for lateral carrier injection into the c-plane QWs. In blue LEDs, V-defects have only a small impact, mainly reducing Vro, by 0.14 V because carriers are rather efficiently injected vertically. This feature cannot be observed without including both random alloy fluctuaion and the V-defect. With considering only the V-defect model [15], carriers can only diffuse into QW through the V-defect where the influence of the Vdefect density might be overestimated. In green LEDs, the large polarization-related barriers hamper vertical transport, so carriers are preferentially injected from V-defects. The forward voltage Vror is strongly reduced by about 1.0 V, even at small V-defect densities, but the limited lateral diffusion length induces current crowding near V-defects. Therefore, increasing the V-defect density increases the peak IQE at large current densities. With the use of an alternative 2D model to 3D models, we could simulate a much larger, realistic area of LEDs and observe the limits of lateral carrier diffusion from V-defects due to random alloy fluctuations, while these features cannot be seen in 3D simulations as the modeled LED size is well below the diffusion length, severely limited by computing resources.

When carriers are injected into the c-plane QWs at high bias and current density, they can screen the polarization field and thereby allow more carriers to be injected either through V-defects or vertically through the c-plane stack of barriers and wells, thus providing a welcome synergy between V-defects and vertical carrier injection. However, optimization will require further work. Although the increase in the V-defect density decreases Vron it also reduces the IQE due to a higher possibility to be trapped and recombine nomadiatively in TDs around the center of V-defects. Detailed measurements of these nomadiative parameters are required for precise selection of the V-defect density and size.

ACKNOWLEDGMENTS

This work is supported by the Ministry of Science and Technology, Taiwan (Grants No. MOST 108-2628-E-002-010-MY3, No. MOST 110-2923-E-002-002, and No. MOST 111-2923-E-002-009). The work at UCSB is supported by the National Science Foundation (Grant No. DMS-1839077), and by grants from the Simons Foundation (Grants No. 601952 to J.S. and No. 601954 to C.W.).

This work is also supported by the TECCLON project, Grant No. ANR-20-CE05-0037-0I of the French Agence Nationale de la Re-cherche (ANR). The data used in this paper can be requested by contacting the corresponding author. The modeling tool was developed by the NTU laboratory, and more detailed information can be found online [48]. Additional support for JSS was provided by the U.S. Department of Energy (Award No. DE-EE0009691).

- [I] C. Weisbuch, On the search for efficient solid state light emitters: Past, present, future, ECS J. Solid State Sci. Technol. 9, 016022 (2019).
- [2] M. Auf der Maur, A. Pecchia, G. Penazzi, W. Rodrigues, and A. Di Carlo, Efficiency Drop in Green lnGaN/GaN Light Emitting Diodes: The Role of Random Alloy Fluctuations, Phys. Rev. Lett. 116, 027401 (2016).
- [3] M. Auf der Maur, D. Barettin, A. Pecchia, F. Sacconi, and A. Di Carlo, in *Numerical Simulation of Optoelectronic Devices*, 2014 (2014), p. 11.
- [4] C. Lynsky, A. I. Alhassan, G. Lheureux, B. Bonef, S. P. DenBaars, S. Nakamura, Y.-R. Wu, C. Weisbuch, and J. S. Speck, Barriers to carrier transport in multiple quantum well nitride-based c-plane green light emitting diodes, Phys. Rev. Mater. 4, 054604 (2020).
- [5] A. H. Mukund, lnGaN/GaN Multiple Quantum Well Light-Emitting Diodes Grown on Polar, Semi-Polar and Non-Polar Orientations (North Carolina State University, Raleigh, NC, U.S.A., 2014).
- [6] G. Lheureux, C. Lynsky, Y.-R. Wu, J. S. Speck, and C. Weisbuch, A 3D simulation comparison of carrier transport in green and blue c-plane multi-quantum well nitride light emitting diodes, J. Appl. Phys. 128, 235703 (2020).
- [7] K. Qwah, M. Monavarian, G. Lheureux, J. Wang, Y.-R. Wu, and J. Speck, Theoretical and experimental investigations of vertical hole transport through unipolar AIGaN structures: Impacts of random alloy disorder, Appl. Phys. Lett. 117, 022107 (2020).
- [8] T.-J. Yang, R. Shivaraman, J. S. Speck, and Y.-R. Wu, The influence of random indium alloy fluctuations in indium gallium nitride quantum wells on the device behavior, J. Appl. Phys. 116, 113104 (2014).
- [9] Y.-R. Wu, R. Shivaraman, K.-C. Wang, and J. S. Speck, Analyzing the physical properties oflnGaN multiple quantum well light emitting diodes from nano scale structure, Appl. Phys. Lett. 101, 083505 (2012).
- [10] H.-H. Chen, J. S. Speck, C. Weisbuch, and Y.-R. Wu, Three dimensional simulation on the transport and quantum efficiency of UVC-LEDs with random alloy fluctuations, Appl. Phys. Lett. 113, 153504 (2018).
- [11] M.A. der Maur, A. Pecchia, and A. Di Carlo, in 2015 IEEE Ist International Forum on Research and Technologies for Society and Industry Leveraging a better tomorrow (RTSI) (IEEE, 2015), p. 153.
- [12] S. Lester, F. A. Ponce, M. G. Craford, and D. A. Steiger-wald, High dislocation densities in high efficiency GaN-based light-emitting diodes, Appl. Phys. Lett. 66, 1249 (1995).

- [13] V. Voronenkov, N. Bochkareva, R. Gorbunov, P. Latyshev, Y. Lelikov, Y. Rebane, A. Tsyuk, A. Zubrilov, and Y. Shreter, Nature of V-shaped defects in GaN, Jpn. J. Appl. Phys. 52, 08JE14 (2013).
- [14] H. Yoshida, T. Hikosaka, H. Nago, and S. Nunoue, Impact of dislocations and defects on the relaxation behavior of lnGaN/GaN multiple quantum wells grown on Si and sapphire substrates, Physica Status Solidi (b) 252, 917 (2015).
- [15] C.-K. Li, C.-K. Wu, C.-C. Hsu, L.-S. Lu, H. Li, T.-C. Lu, and Y.-R. Wu, 3d numerical modeling of the carrier transport and radiative efficiency for ingan/gan light emitting diodes with v-shaped pits, AlP Adv. 6, 055208 (2016).
- [16] Y.-H. Cho, 1.-Y. Kim, J. Kim, M.-B. Shim, S. Hwang, S.-H. Park, Y.-S. Park, and S. Kim, Quantum efficiency affected by localized carrier distribution near the V-defect in GaN based quantum well, Appl. Phys. Lett. 103, 261101 (2013).
- [17] Z. Quan, J. Liu, F. Fang, G. Wang, and F. Jiang, Effect of V-shaped pit area ratio on quantum efficiency of blue lnGaN/GaN multiple-quantum well light-emitting diodes, Opt. Quantum Electron. 48, 195 (2016).
- [18] H.-T. Shen, C. Weisbuch, J. S. Speck, and Y.-R. Wu, Three-Dimensional Modeling of Minority-Carrier Lateral Diffusion Length Including Random Alloy Fluctuations in (In, Ga) N and (Al, Ga) N Single Quantum Wells, Phys. Rev. Appl. 16, 024054 (2021).
- [19] S. Zhou and X. Liu, Effect of V-pits embedded InGaN/GaN superlattices on optical and electrical properties of GaN-based green light-emitting diodes, Physica Status Solidi (a) 214, 1600782 (2017).
- [20] X. Wu, C. Elsass, A. Abare, M. Mack, S. Keller, P. Petroff, S. DenBaars, J. Speck, and S. Rosner, Structural origin of V-defects and correlation with localized excitonic centers in lnGaN/GaN multiple quantum wells, Appl. Phys. Lett. 72, 692 (1998).
- [21] Y.-L. Hu, R. M. Farrell, C. J. Neufeld, M. Iza, S. C. Cruz, N. Pfaff, D. Simeonov, S. Keller, S. Nakamura, S. P. Den-Baars, U. K. Mishra, and J. S. Speck, Effect of quantum well cap layer thickness on the microstructure and performance of lnGaN/GaN solar cells, Appl. Phys. Lett. 100, 161101 (2012).
- [22] A. Romanov, T. Baker, S. Nakamura, J. Speck, and E. U. Group, Strain-induced polarization in wurtzite III-nitride semipolar layers, J. Appl. Phys. 100, 023522 (2006).
- [23] F. Jiang, J. Zhang, L. Xu, J. Ding, G. Wang, X. Wu, X. Wang, C. Mo, Z. Quan, X. Guo, C. Zheng, S. Pan, and J. Liu, Efficient lnGaN-based yellow-light-emitting diodes, Photonics Res. 7, 144 (2019).
- [24] C. Lynsky, R. C. White, Y. C. Chow, W. Y. Ho, S. Nakamura, S. P. DenBaars, and J. S. Speck, Role of V-defect density on the performance of III-nitride green LEDs on sapphire substrates, J. Cryst. Growth 560, 126048 (2021).
- [25] S.-H. Han, D.-Y. Lee, H.-W. Shim, J. Wook Lee, D.-J. Kim, S. Yoon, Y. Sun Kim, and S.-T. Kim, Improvement of efficiency and electrical properties using intentionally formed V-shaped pits in lnGaN/GaN multiple quantum well light-emitting diodes, Appl. Phys. Lett. 102, 251123 (2013).

- [26] C. Ren, B. Rouet-Leduc, J. Griffiths, E. Bohacek, M. Wallace, P. Edwards, M. Hopkins, D. Allsopp, M. Kappers, R. Martin, and R. Oliver, Analysis of defect-related inhomogeneous electroluminescence in lnGaN/GaN QW LEDs, Superlattices Microstruct. 99, 118 (2016).
- [27] R. Bouveyron, M. Mrad, and M. Charles, V-pit pinning at the interface of high and low-temperature gallium nitride growth, Jpn. J. Appl. Phys. **58**, SC1035 (2019).
- [28] A. Di Vito, A. Pecchia, A. Di Carlo, and M. Auf der Maur, Simulating random alloy effects in III-nitride light emitting diodes, J. Appl. Phys. **128**, 041102 (2020).
- [29] M. Filoche, M. Piccardo, Y.-R. Wu, C.-K. Li, C. Weisbuch, and S. Mayboroda, Localization landscape theory of disorder in semiconductors. I. Theory and modeling, Phys. Rev. B95, 144204 (2017).
- [30] M. Piccardo, C.-K. Li, Y.-R. Wu, J. S. Speck, B. Bonef, R. M. Farrell, M. Filoche, L. Martinelli, J. Peretti, and C. Weisbuch, Localization landscape theory of disorder in semiconductors. ii. urbach tails of disordered quantum well layers, Phys. Rev. B 95, 144205 (2017).
- [31] C.-K. Li, M. Piccardo, L.-S. Lu, S. Mayboroda, L. Martinelli, J. Peretti, J. S. Speck, C. Weisbuch, M. Filoche, and Y.-R. Wu, Localization landscape theory of disorder in semiconductors. III. Application to carrier transport and recombination in light emitting diodes, Phys. Rev. B 95, 144206 (2017).
- [32] D. N. Arnold, G. David, D. Jerison, S. Mayboroda, and M. Filoche, Effective Confining Potential of Quantum States in Disordered Media, Phys. Rev. Lett. 116, 056602 (2016).
- [33] M. Filoche and S. Mayboroda, Universal mechanism for anderson and weak localization, Proc. National Acad. Sci. 109, 14761(2012).
- [34] E. Kioupakis, P. Rinke, K. T. Delaney, and C. G. Van de Walle, Indirect auger recombination as a cause of efficiency droop in nitride light-emitting diodes, Appl. Phys. Lett. 98, 161107 (2011).
- [35] L. C. Le, D. G. Zhao, D. S. Jiang, L. Li, L. L. Wu, P. Chen, Z. S. Liu, Z. C. Li, Y. M. Fan, J. J. Zhu, H. Wang, S. M. Zhang, and H. Yang, Carriers capturing of V-defect and its effect on leakage current and electroluminescence in lnGaN-based light-emitting diodes, Appl. Phys. Lett. 101, 252110 (2012).
- [36] X. Wu, J. Liu, Z. Quan, C. Xiong, C. Zheng, J. Zhang, Q. Mao, and F. Jiang, Electroluminescence from the sidewall quantum wells in the V-shaped pits oflnGaN light emitting diodes, Appl. Phys. Lett. 104, 221101 (2014).
- [37] M. Shiojiri, C. Chuo, J. Hsu, J. Yang, and **H.** Saijo, Structure and formation mechanism of V defects in multiple In Ga N/ Ga N quantum well layers, J. Appl. Phys. 99, 073505 (2006).
- [38] C.-Y. Chang, H. Li, Y.-T. Shih, and T.-C. Lu, Manipulation ofnanoscale V-pits to optimize internal quantum efficiency of lnGaN multiple quantum wells, Appl. Phys. Lett. 106, 091104 (2015).
- [39] S. Tomiya, Y. Kanitani, S. Tanaka, T. Ohkubo, and K. Hono, Atomic scale characterization of GalnN/GaN multiple quantum wells in V-shaped pits, Appl. Phys. Lett. 98, 181904 (2011).
- [40] S. Zhou, X. Liu, H. Yan, Y. Gao, H. Xu, J. Zhao, Z. Quan, C. Gui, and S. Liu, The effect of nanometre-scale V-pits

- on electronic and optical properties and efficiency droop of GaN-based green light-emitting diodes, Sci. Rep. 8, 1 (2018).
- [41] K. Kumakura, T. Makimoto, N. Kobayashi, T. Hashizume, T. Fukui, and H. Hasegawa, Minority carrier diffusion length in GaN: Dislocation density and doping concentration dependence, Appl. Phys. Lett. 86, 052105 (2005).
- [42] S. Y. Karpov and Y. N. Mak:arov, Dislocation effect on light emission efficiency in gallium nitride, Appl. Phys. Lett. 81, 4721(2002).
- [43] C. A. Robertson, K. S. Qwah, Y.-R. Wu, and J. S. Speck, Modeling dislocation-related leakage currents in GaN p-n diodes, J. Appl. Phys. 126, 245705 (2019).

- [44] K. S. Qwah, C. A. Robertson, Y.-R. Wu, and J. Speck, Modeling dislocation-related reverse bias leakage in GaN p-n diodes, Semicond. Sci. Technol. (2021).
- [45] H.-Y. Ryu, H.-S. Kim, and J.-1. Shim, Rate equation analysis of efficiency droop in lnGaN light-emitting diodes, Appl. Phys. Lett. 95, 081114 (2009).
- [46] C. Wang, Y. Chiou, and H. Chang, Investigating the efficiency droop of nitride-based blue LEDs with different quantum barrier growth rates, Crystals 9, 677 (2019).
- [47] Y. Li, W. Tang, Y. Zhang, M. Guo, Q. Li, X. Su, A. Li, and F. Yun, Nanoscale characterization of V-defect in lnGaN/GaN QWs LEDs using near-field scanning optical microscopy, Nanomaterials 9,633 (2019).
- [48] http://yrwu-wk.ee.ntu.edu.tw/.